Extracting information on the spatial variability in erosion rate stored in detrital cooling age distributions in river sands

Jean Braun[1], Lorenzo Gemignani[2], and Peter van der Beek[3]

[1]GFZ German Research Centre for Geosciences, Telegrafenberg 14473, Potsdam, Germany
[2]Department of Earth Sciences, Cluster Geology and Geochemistry, Vrij Universiteit Amsterdam, The Netherlands
[3] ISTerre, Université Grenoble Alpes and CNRS, CS 40700, 38058 Grenoble Cedex 9, France

Correspondence to: J. Braun (jbraun@gfz-potsdam.de)

Abstract. The purpose of detrital thermochronology is to provide constraints on regional scale exhumation rate and its spatial variability in actively eroding mountain ranges. Procedures that use cooling age distributions coupled with hypsometry and thermal models have been developed in order to extract quantitative estimates of erosion rate and its spatial distribution, assuming steady state between tectonic uplift and erosion. This hypothesis precludes the use of these procedures to assess the

5 likely transient response of mountain belts to changes in tectonic or climatic forcing. In this paper, we describe a simple method that, using the observed detrital mineral age distributions collected in a system of river catchments, allows to extract information about the relative distribution of erosion rates in an eroding hinterland without relying on a steady-state assumption or the value of thermal parameters. The model is based on a relatively low number of parameters describing lithological variability among the various catchments and their sizes, and only uses the raw binned ages. In order to illustrate the method, we invert age

10 distributions collected in the Eastern Himalaya, one of the most tectonically active places on Earth. From the inversion of the cooling age distributions we predict present day erosion rates of the catchments along the Siang-Tsangpo-Brahmaputra river system, as well as smaller tributaries. We show that detrital age distributions contain dual information about present-day erosion rate, i.e. from the predicted distribution of surface ages within each catchment and from the relative contribution of any given catchment to the river distribution. The inversion additionally allows comparing modern erosion rates to long-term

15 exhumation rates. We provide a simple implementation of the method in R.code within a Jupyter Notebook that includes the data used in this paper for illustration purposes.

1 Introduction

Thermochronometric methods provide us with estimates of the cooling age of a rock, i.e. the time in the past when the rock cooled through a so-called closure temperature (Dodson, 1973), which varies between systems and minerals. One of the main geological processes through which rocks experience cooling is exhumation towards the cold, quasi-isothermal surface (Brown, 1991). Young ages are commonly interpreted to indicate rapid exhumation and old ages should correspond to slow exhumation. Cooling ages can also record more discrete cooling events such as the nearby emplacement of hot intrusions (Gleadow and Brooks, 1979) or the rapid relaxation of isotherms at the end of an episode of rapid erosion (Braun, 2016).

Datasets are now routinely assembled by collecting and dating a large number of mineral grains from a sand sample collected at a given location in a river draining an actively eroding area. Such detrital thermochronology datasets provide a proxy for the distribution of surface rock ages in a given catchment (Bernet et al., 2004; Brandon, 1992). By repeating this operation at different sites along a river stream, one obtains redundant information that can be used to document more precisely the spatial variability of in-situ thermochronological ages in a river catchment (Bernet et al., 2004; Brewer et al., 2006).

Methods have been devised to extract quantitative information from such detrital datasets concerning the erosion history of a tectonically active area, as well as estimates of its spatial variability. Ruhl and Hodges (2005) convolved their detrital age datasets with the hypsometry of the catchment to test the assumption of topographic steady-state in a rapidly eroding catchment of Nepalese Himalaya. Similarly, Stock et al. (2006) and Vermeesch (2007) combined detrital apatite (U-Th)/He age datasets with an age-elevation relationship established from in-situ samples to predict the distribution of present-day erosion rates in the eastern Sierra Nevada and White Mountains of California, respectively. Whipp et al. (2009) used simulations from a thermo-kinematic model to define the limits of applicability of such a technique, while Enkelmann and Ehlers (2015) used it in a glaciated landscape. Wobus et al. (2003, 2006) collected samples from tributaries of the Burhi Gandaki and Trisuli rivers to document the strong transition in erosion rate across a major topographic transition. By limiting their sampling to tributaries, they circumvented the need to develop and use a mixing model for the interpretation of their data. Brewer et al. (2006) derived optimal values for erosion rate in neighbouring catchments by comparing and mixing theoretical probability density distributions with detrital age data from the Marsyandi River in Nepal. More recently, McPhillips and Brandon (2010) used detrital cooling ages combined with in-situ age measurements to infer a recent increase in relief in the Sierra Nevada, California.

However, these methods have not taken advantage of the fact that detrital age distributions contain two separate pieces of information concerning the spatial patterns of present and past rates of erosion. The first piece of information comes from the ages themselves: catchments or sub-catchments where the proportion of grains with young ages dominates are likely to experience rapid exhumation today or in the recent past; whereas catchments or sub-catchments where the proportion of grains with old ages dominates are more likely to have experienced rapid erosion in a more distant past. However, there does not need to be a one-to-one correlation between young ages and fast present-day erosion rate or old ages and low present-day erosion rate, as a rapidly exhuming catchment may not have experienced sufficient total erosion to exhume rocks bearing reset ages.

Alternatively regions that produce relatively young ages may have experienced a step decrease in erosion rate in the recent past.

The second source of information comes from the mixing that takes place in the river. For this, ages can be regarded as passive markers (or colors) that inform us on the proportion in which the mixing takes place today, which is directly proportional to

5 the present-day erosion rate. Using this information, the fastest present-day erosion rates should be predicted where the age distributions change along the river/stream, everything else being accounted for, such as the relative size of neighbouring sub-catchments or the potential change in lithology between them. Here we propose that combining the two sources of information should tell us more about the present-day erosion rate and, as we will show, about its antiquity.

To demonstrate this point, we have devised a simple method that, unlike many others such as that of Brewer et al. (2006),

10 is only dependent on the raw, binned age data. This avoids any complication or bias that may arise from trying to compare the data to theoretical probability density distributions that rely on a thermal model prediction. We recognise the value of doing so, but thermal models require making assumptions about past geothermal gradient (heat flux), or rock thermal conductivity and heat production, which introduces additional uncertainty in interpreting the data. The first part of this paper describes the method.

15 Due to its relative simplicity, our method is, however, strongly limited by the quality and representativeness of the measured age distributions, i.e. whether samples of 30 to 100 grains are representative of the age distribution of an entire catchment. To test the robustness of our predictions, we have used a simple bootstrapping algorithm that yields uncertainty estimates on the derived erosion rates. This is briefly explained in the second part of the paper.

To demonstrate the ease of use, applicability and usefulness of our new method, we have applied it to several datasets

20 collected in the Himalaya (along the Tsangpo-Siang-Brahmaputra river system). This is explained in the third part of the paper. There we show that the method yields reliable estimates of the distribution of present-day erosion rates in these areas as well as independent information on the spatial extent of past geological events.

2 The method

2.1 Basic assumptions

25 We assume that we have collected a series of age datasets measured at M specific points (or sites) along a river that drains a tectonically active regions where erosion rate is likely to vary spatially. We also assume that the datasets have been used to construct ages distributions decomposed into N age *bins* that may, for example, correspond to given, known geological events or, alternatively, have been selected without prior knowledge, usually uniformly distributed and of equal age width over a given age range, i.e. the range of observed ages (see Figure 1). Although each bin corresponds to an age range, it might be easier to

30 refer to it as representative of an event of a given "age" which can be taken as the mean age of the range, for example. We will call H_i^k for $k = 1, \cdots, N$ and $i = 1, \cdots, M$ the relative height of bin k in distribution i. Because these are relative contributions,

we have:

$$\sum_{k=1}^{N} H_i^k = 1, \quad \text{for all } i = 1, \cdots, M \tag{1}$$

Example of measured age distribution
$N = 4$
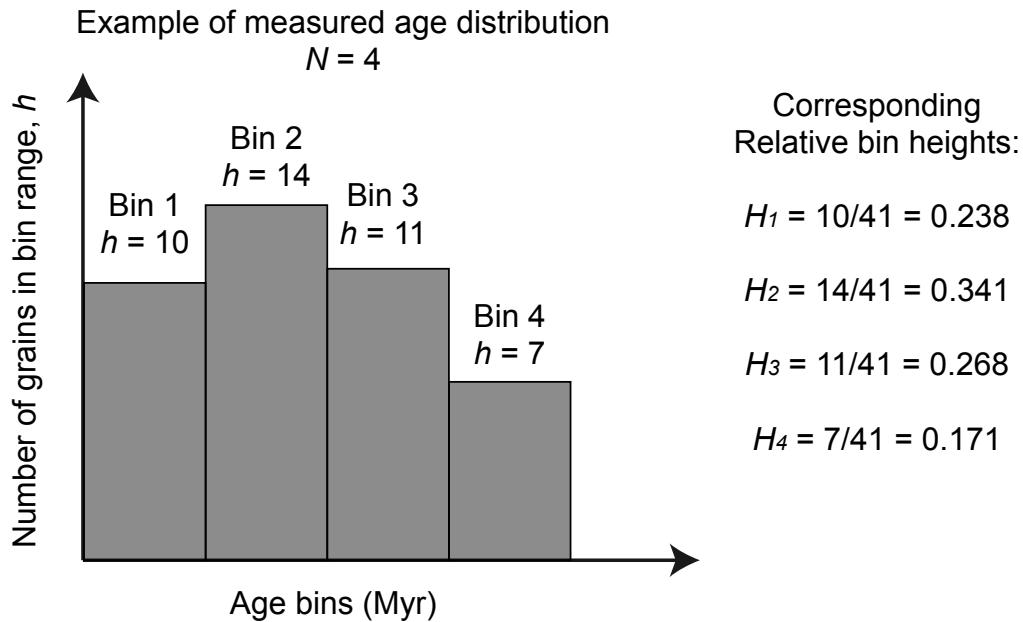
Figure 1. Example of a measured age distribution and the relative heights H_i^k of the corresponding bins ($N = 4$ in this example).

The landscape is divided into *exclusive* contributing areas for each of the points along the main river where we have measured

5 a dataset and compiled from it a distribution. We take the convention that Area 1 (of surface area A_1) is the area contributing to site 1, whereas Area 2 (of surface area A_2) is the area contributing to site 2 but not to site 1. Area i (of surface area A_i) therefore contributes to site i but not to the previous $i - 1$ sites (see Figure 2). In each Area i, we will assume that α_i is the relative abundance of the mineral used to estimate the age distribution in rocks being eroded from the surface. We take the convention that $0 < \alpha_i < 1$, with $\alpha_i = 1$ corresponding to an area i with surface rocks that contain the mineral in abundance

10 (for example granite for muscovite) and $\alpha_i = 0$ corresponding to an area i with surface rocks that do not contain the mineral (for example carbonates for muscovite). If, for example, the area is made of 60% granite and 40% carbonates, and we have measured ages using a mineral that is abundant in granites (like muscovite) but absent in carbonates, then $\alpha = 0.6$. We also call ϵ_i the unknown present-day mean erosion rate in Area i.

The surface areas, A_i, can be computed from a Digital Elevation Model. The value of the concentration factors is critical;

15 constraining them depends on the regional geology and available data. A first-order approximation of the concentration factors
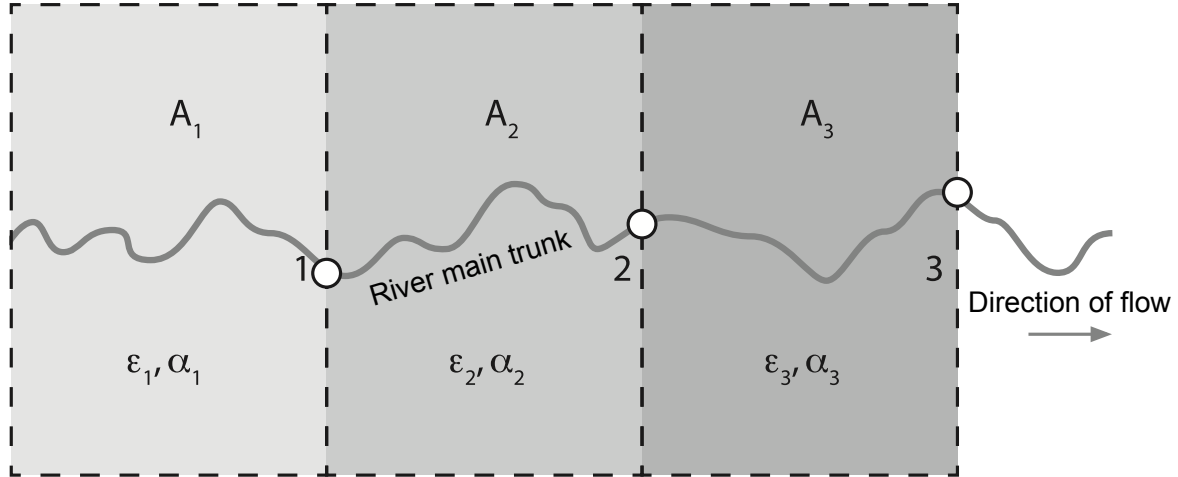
Figure 2. Schematic representation of how the landscape is divided into exclusive contributing areas A_i (different shades of grey) for each of the points (here the circles labeled $i = 1, \cdots, 3$) along the main river where we have age distributions. ϵ_i and α_i are the assumed mean erosion rate and surface rock mineral density of area i, respectively.

or 'fertility', α_i, can be derived from a geological map or from the relative concentration of given minerals in each of the samples used to derive the age distributions, by using the method described in Malusà et al. (2016), for example.

From these simple assumptions, we can then write that the number of grains of age k coming out of catchment i is given by:

$$D_i^k = A_i \epsilon_i \alpha_i C_i^k \tag{2}$$

where C_i^k is the unknown relative concentration of grains of age k in surficial rocks in Area i. We also have:

$$\sum_{k=1}^{N} C_i^k = 1, \quad \text{for all } i \tag{3}$$

because the C_i^k are also relative or normalized concentrations. The relative concentrations, C_i^k tells us if the event corresponding to age k has affected Area i (or, more correctly, if it has been preserved in its surficial rocks) whereas ϵ_i is a measure of
10 present-day erosion rate in Area i.

2.2 Downstream bin summation along main trunk

We can now write that the predicted height of bin k in the distribution observed at site i should be equal to the total number of grains of age bin k coming from all upstream areas divided by the total number of grains of all ages coming from all upstream areas:

$$H_i^k = \left(\sum_{j=1}^{i} D_j^k\right) / \left(\sum_{k=1}^{N}\sum_{j=1}^{i} D_j^k\right) = \left(\sum_{j=1}^{i} A_j \epsilon_j \alpha_j C_j^k\right) / \left(\sum_{k=1}^{N}\sum_{j=1}^{i} A_j \epsilon_j \alpha_j C_j^k\right) \tag{4}$$

We can slightly re-arrange this to obtain:

$$H_i^k = \Big(\sum_{j=1}^{i} A_j \epsilon_j \alpha_j C_j^k\Big) / \Big(\sum_{j=1}^{i} A_j \epsilon_j \alpha_j \sum_{k=1}^{N} C_j^k\Big) = \Big(\sum_{j=1}^{i} A_j \epsilon_j \alpha_j C_j^k\Big) / \Big(\sum_{j=1}^{i} A_j \epsilon_j \alpha_j\Big) \tag{5}$$

If we divide the numerator and denominator of this expression by $A_1 \epsilon_1 \alpha_1$, we obtain:

$$H_i^k = \sum_{j=1}^{i} \rho_j C_j^k / \sum_{j=1}^{i} \rho_j \tag{6}$$

where:

$$\rho_j = \frac{A_j \epsilon_j \alpha_j}{A_1 \epsilon_1 \alpha_1} \tag{7}$$

is the contribution from Area j relative to Area 1. Note that, if we assume that we can confidently estimate A_j and α_j, ρ_j becomes a measure of the unknown erosion rate, ϵ_j, in Area j relative to the unknown erosion rate, ϵ_1, in Area 1.

2.3 Incremental formulation

We now try to express Equation (6) as an incremental relationship between H_i^k and H_{i-1}^k only, i.e. between the relative bin heights between distributions measured at two successive points along the main trunk. From Equation (6), we can write:

$$H_i^k = \sum_{j=1}^{i} \rho_j C_j^k / \sum_{j=1}^{i} \rho_j = \Big(\sum_{j=1}^{i-1} \rho_j C_j^k + \rho_i C_i^k\Big) / \Big(\sum_{j=1}^{i-1} \rho_j + \rho_i\Big) \tag{8}$$

and by dividing numerator and denominator by $\sum_{j=1}^{i-1} \rho_j$, we obtain:

$$H_i^k = \big(H_{i-1}^k + \delta_i C_i^k\big) / \big(1 + \delta_i\big) \tag{9}$$

where:

$$\delta_i = \rho_i / \sum_{j=1}^{i-1} \rho_j \tag{10}$$

We can finally write:

$$H_i^k - H_{i-1}^k = (C_i^k - H_i^k)\delta_i \tag{11}$$

From this relationship we see that the relative changes in bin height between two successive sites along the main stream tells us something about the present-day erosion rate in the intervening catchment. However, if the relative bin heights do not change between two successive sites ($H_i^k = H_{i-1}^k$), then we cannot tell if this is because the erosion rate in catchment i is nil ($\epsilon_i = 0 \rightarrow \rho_i = 0 \rightarrow \delta_i = 0$), or because the signature of the source in catchment i, i.e. the distribution of ages at the surface, is identical to that of the previous catchment ($C_i^k = H_i^k = H_{i-1}^k$).

2.4 Inverting for C_i^k and ϵ_i

Using Equation (11), we can now obtain the unknown C_i^k recursively using:

$$C_i^k = \frac{H_i^k - H_{i-1}^k}{\delta_i} + H_i^k \tag{12}$$

by making first the simplest assumption that $\epsilon_i = \epsilon_1$ for all i, which leads to:

$$\rho_i = \frac{A_i \alpha_i}{A_1 \alpha_1} \tag{13}$$

and

$$\delta_i = A_i \alpha_i / \sum_{j=1}^{i-1} A_j \alpha_j \tag{14}$$

Assuming a uniform erosion rate ($\epsilon_i = \epsilon_1$) should be regarded as the zeroth-order scenario that should first be considered to explain the data; it may, however, lead to unrealistic solutions for any of the C_i^k, i.e. values of C_i^k that are not in the range $[0,1]$. To avoid this we must add two conditions that affect the values for the unknown δ_i. $C_i^k > 0$ implies that:

$$\delta_i > \frac{H_{i-1}^k - H_i^k}{H_i^k} \quad \text{for all } k = 1, \cdots, N \tag{15}$$

and $C_i^k < 1$ implies, in turn, that:

$$\delta_i > \frac{H_i^k - H_{i-1}^k}{1 - H_i^k} \quad \text{for all } k = 1, \cdots, N \tag{16}$$

The first condition applies where there is a decrease in any relative bin height k between locations $i-1$ and location i, i.e. $H_i^k < H_{i-1}^k$, whereas the second condition applies where there is an increase in any relative bin height k between locations $i-1$ and i, i.e. $H_i^k > H_{i-1}^k$. We make the further (and trivial) assumption that the true erosion rate must satisfy both conditions.

2.5 Procedure summary for main trunk distributions

To obtain estimates of erosion rate in each catchment, we then proceed sequentially for $i = 1, \cdots, M$, where M is the number of locations within the river where we have an age distribution. For each site i, we first compute δ_i according to:

$$\delta_i = \max_{k=1,\cdots,N} \left(A_i \alpha_i / \sum_{j=1}^{i-1} A_j \alpha_j, \frac{H_{i-1}^k - H_i^k}{H_i^k}, \frac{H_i^k - H_{i-1}^k}{1 - H_i^k} \right) \tag{17}$$

From this value of δ_i, we can deduce an erosion rate (relative to the erosion rate in the first catchment, ϵ_1) from:

$$\epsilon_i = \frac{\delta_i}{A_i \alpha_i} \sum_{j=1}^{i-1} A_j \alpha_j \epsilon_j \tag{18}$$

as well as the relative concentration of grains of age in bin k in Area A_i, using:

$$C_i^k = \frac{H_i^k - H_{i-1}^k}{\delta_i} + H_i^k \tag{19}$$

for all $k = 1, \cdots, N$. For the first catchment, i.e. $i = 1$, we assume that $\epsilon_1 = 1$ and $C_i^k = H_i^k$.

3 Using age distributions from tributaries

Age distributions from tributaries can be included to improve the solution locally, i.e. in the catchment that includes the tributary. Let's call A_T, α_t and ϵ_T the catchment area, the abundance of the target mineral in surface rocks and the mean erosion rate of the catchment of the tributary, and A_M, α_M and ϵ_M the catchment area, the abundance of the target mineral in surface rocks and the mean erosion rate of the rest of catchment A_i.

For each bin k in the catchment i, we can write:

$$A_i \epsilon_i \alpha_i C_i^k = A_T \epsilon_T \alpha_T C_T^k + A_M \epsilon_M \alpha_M C_M^k \tag{20}$$

By conservation of eroded rock mass, we have:

$$A_M \epsilon_M \alpha_M = A_i \epsilon_i \alpha_i - A_T \epsilon_T \alpha_T \tag{21}$$

which we can use to transform Equation (20) into:

$$A_i \epsilon_i \alpha_i C_i^k = A_T \epsilon_T \alpha_T C_T^k + (A_i \epsilon_i \alpha_i - A_T \epsilon_T \alpha_T) C_M^k \tag{22}$$

to obtain:

$$C_M^k = \frac{A_i \epsilon_i \alpha_i C_i^k - A_T \epsilon_T \alpha_T C_T^k}{A_i \epsilon_i \alpha_i - A_T \epsilon_T \alpha_T} \tag{23}$$

Using the method for the main trunk data described in the previous sections, we know ϵ_i and C_i^k. The tributary data (age distributions) gives us the C_T^k ($C_T^k = H_T^k$ because ...) and we can solve for the C_M^k assuming first that the erosion rate is uniform in the catchment i, i.e. $\epsilon_T = \epsilon_M = \epsilon_i$, to give:

$$C_M^k = \frac{A_i \alpha_i C_i^k - A_T \alpha_T C_T^k}{A_i \alpha_i - A_T \alpha_T} \tag{24}$$

However, this may lead to unrealistic values of the C_M^k, i.e. not comprised between 0 and 1. Consequently, two conditions need to be added so that $0 < C_M^k < 1$ for all k which might yield to erosion rate estimate in the tributary catchment, ϵ_T, different from ϵ_i obtained for A_i. The first condition ($C_M^k > 0$) yields:

$$\epsilon_T < \frac{A_i \alpha_i C_i^k}{A_T \alpha_T C_T^k} \epsilon_i \tag{25}$$

while the second condition ($C_M^k < 1$) yields:

$$\epsilon_T < \frac{A_i \alpha_i (1 - C_i^k)}{A_T \alpha_T (1 - C_T^k)} \epsilon_i \tag{26}$$

The true erosion rate must satisfy both conditions and we therefore select the smallest value of ϵ_T obtained by considering any relative surface concentration difference between the tributary sub-catchment concentration (C_T^k) and that of the entire catchment (C_i^k).

3.1 Procedure summary for tributary distributions

In summary, we first compute the erosion rate in the sub-catchment of the tributary, according to:

$$\epsilon_T = \min_{k=1,\cdots,N} \left(\epsilon_i, \frac{A_i \alpha_i C_i^k}{A_T \alpha_T C_T^k} \epsilon_i, \frac{A_i \alpha_i (1 - C_i^k)}{A_T \alpha_T (1 - C_T^k)} \epsilon_i \right) \tag{27}$$

and we then use it to compute the C_M^k according to:

$$C_M^k = \frac{A_i \epsilon_i \alpha_i C_i^k - A_T \epsilon_T \alpha_T C_T^k}{A_i \epsilon_i \alpha_i - A_T \epsilon_T \alpha_T} \tag{28}$$

from the values of C_i^k and ϵ_i obtained from the trunk data analysis and the C_T^k obtained form the measured distribution in the tributary.

If there are more than one tributary in a catchment, we repeat the operation for each tributary, using the previously computed ϵ_i and C_i^k from the main trunk analysis, under the assumption that the tributaries have disconnected drainage areas in the catchment i.

4 Uncertainty estimates by bootstrapping

We assess the uncertainty of our estimates of erosion rate ϵ_i and relative concentrations C_i^k, by bootstrapping. For this, we simply use the method described above on a large number of sub-samples of the observed distributions constructed by arbitrarily and randomly removing 25% of the observed age estimates. This yields distributions of erosion rate and relative concentrations that can be used to estimate the uncertainty arising from the finite sample size. These distributions are usually not normal and we use their modal value, rather than their mean, as the most likely estimate of erosion rate and their standard deviation to represent uncertainty.

The code is provided as a Jupyter Notebook containing R-code and explanatory notes that refer to the equations given in this manuscript. The user must provide a series of input files containing (a) the description of the sites, i.e. the order in which the sites are located along the river, whether they drain into the main river stem or into a tributary, the drainage area A, the lithological factor α, (b) the bin sizes and (c) the observed age data at each site. The code produces estimates of erosion rate and relative concentration of grains of ages within each range, their mean value, standard deviation and modal values (from the bootstrapping).

5 Applications to detrital age distributions

To illustrate the method, we now apply it to a detrital age datasets from the Eastern Himalaya. The ages correspond to cooling ages, i.e. the time in the past when the rocks cooled through a given closure temperature. The datasets that we use contain ages that were obtained using the muscovite ^{40}Ar/^{39}Ar thermochronometer, which has a closure temperature $T_c \approx 385 \pm 70°$C (Hames and Bowring, 1994), depending on grain size, chemistry, and cooling rate.

Table 1. Age bins used to construct age distributions shown in Figure 4 and used in our example.

Bin 1	Bin2	Bin 3	Bin 4	Bin 5
0-5 Ma	5-10 Ma	10-20 Ma	20-50 Ma	50-500 Ma

Table 2. Relative position along the main trunk of the Tsangpo-Siang-Brahmaputra river system. Negative numbers indicate samples collected along a tributary. Catchment areas and lithological factors used to compute the erosion rate reported in Table 3. Site names refer to locations shown in Figure 3.

Site	Position	Catchment area (km^2)	Lithological factor	Reference
TG-40a	1	55395	0.01	Bracciali et al. (2016)
TG-41a	2	13265	0.03	Bracciali et al. (2016)
A	3	41374	0.0135	Lang et al. (2016)
Y	-4	1250	0.013	Lang et al. (2016)
B	5	2092	0.013	Lang et al. (2016)
X	-6	2135	0.011	Lang et al. (2016)
C	7	1451	0.0123	Lang et al. (2016)
Z	8	111706	0.0131	Bracciali et al. (2016)

Age distributions were constructed from published age datasets collected along the main trunk of the Tsangpo-Siang-Brahmaputra river system, as well as along some of its tributaries (Figure 3), using age bins given in Table 1. Samples A,B,C (composite sample), X and Y are from Lang et al. (2016) and samples Z, T-40a and T-41a are from Bracciali et al. (2016). The complete age datasets are given in the Data Repository, Table S1. In Table 2, we give the relative position of the successive samples along the main trunk of the river, i, the respective exclusive contributing areas, A_i and the lithological factor, α_i, (or abundances of target mineral in surface rocks).

Results are shown in Table 3 as computed relative erosion rates (i.e. normalized such that the mean erosion rate is 1), standard deviations and modal values. Figure 5 contains maps of the various catchments shaded according to their predicted modal erosion rate and concentrations of grains of age within each range, obtained from the bootstrapping and mixing algorithms described above. Predicted concentrations are scaled such that the sum of the five age bin concentrations is 1 in each catchment. We see that predicted erosion rates increase with distance along the main river trunk from its source area along the southern margin of the Tibetan Plateau. Maximum erosion rates are observed in catchment C that is closest to the eastern Himalayan syntax. Further downstream (catchment Z), the predicted erosion rate remains high but lower than observed near the syntax. Interestingly, there is a good correspondence between present-day erosion rate and where the youngest ages are being generated (compare upper left panel showing relative concentration of youngest age bin, to central panel showing predicted present-day erosion rate), with the notable exception of the most downstream catchment (Z). In other words, where the mixing analysis predicts high erosion rate to account for a substantial change in the age distribution between two adjacent catchments, is also
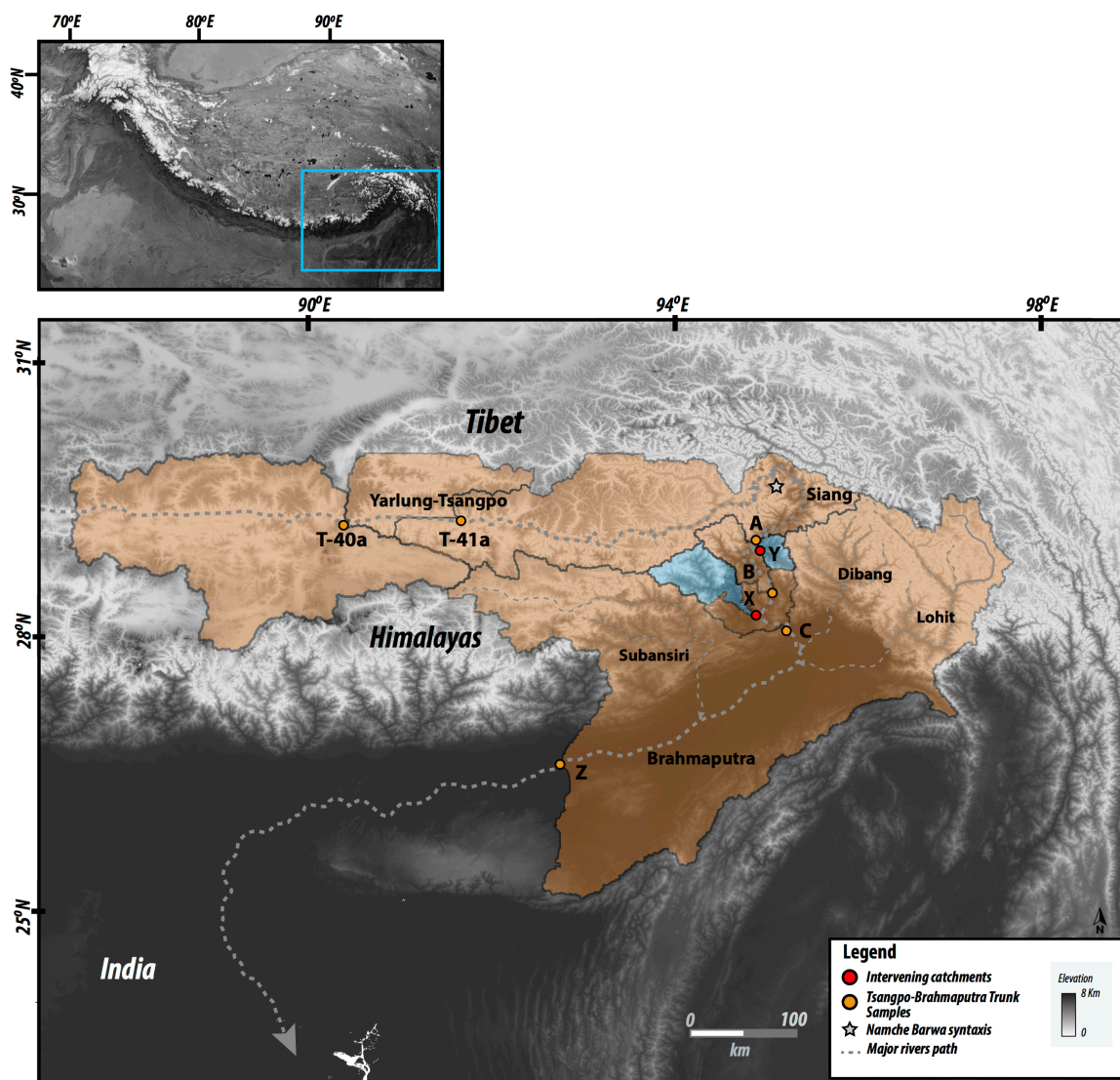
Figure 3. a) Location of the study area and b) location and name of sampling sites and geometry of the drainage basins contributing to each site. The orange shading represents catchments draining directly into the main trunk; pale blue shading represents the tributary catchments or sub-catchments.
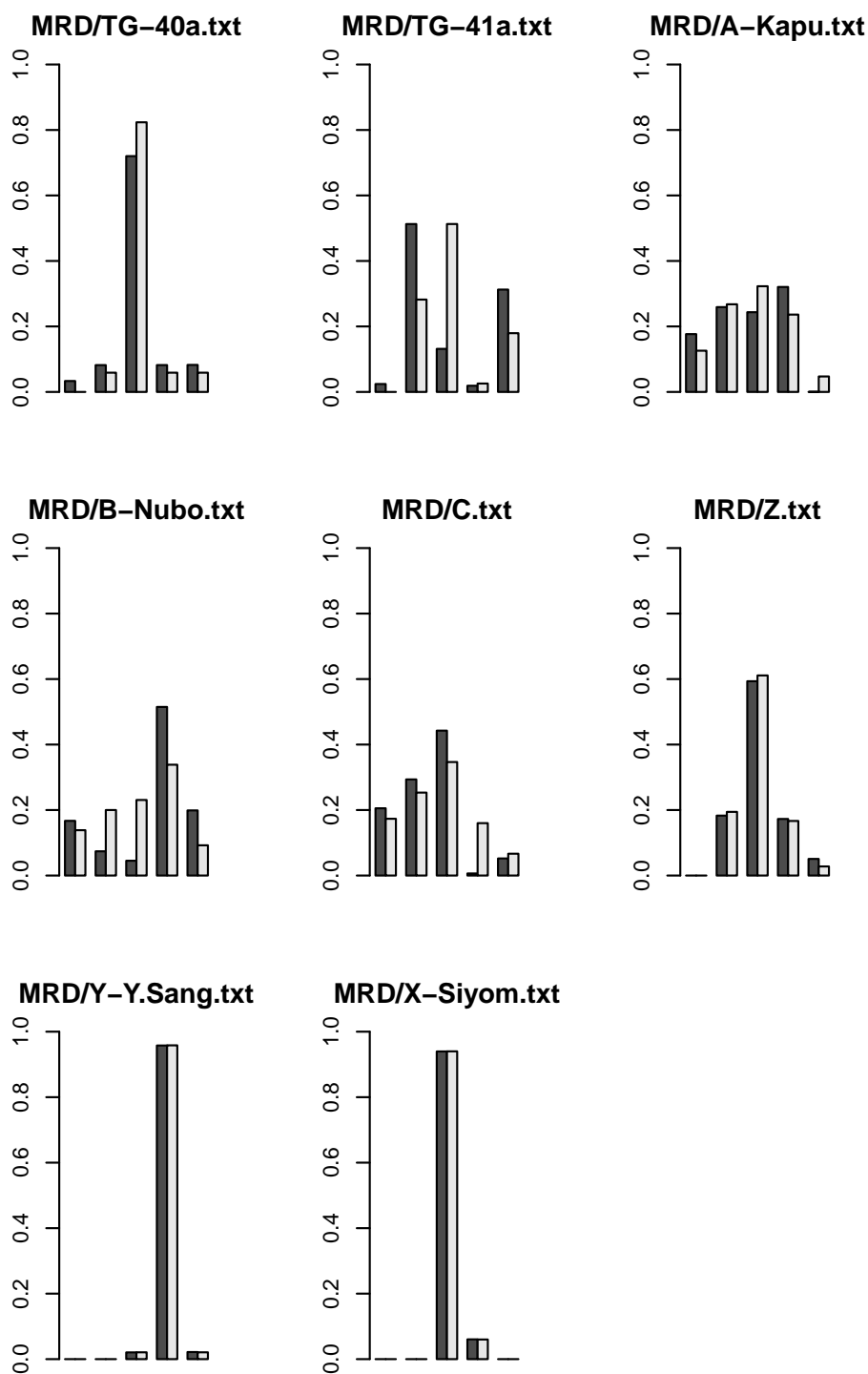
Figure 4. Observed distributions of ages (light grey bars) in samples collected at sites shown in Figure 3 and predicted surface age distributions (dark grey bars) in corresponding catchment areas. Data and results are shown for the sites along the main trunk only.

Table 3. Computed relative erosion rates, variance and modal values obtained from the mixing model and the bootstrapping procedure. Values are normalized such that the mean is 1. Site names refer to locations shown in Figure 3.

Site	Mean erosion rate (mm/yr)	St. deviation (mm/yr)	Modal value (mm/yr)
TG-40a	0.012	0.000	0.012
TG-41a	0.017	0.011	0.012
A	0.059	0.031	0.040
Y	0.92	0.56	0.60
B	0.92	0.56	0.60
X	0.48	0.27	0.31
C	4.5	2.9	2.8
Z	0.48	0.27	0.31

where it predicts the highest concentration of young ages in the surface rocks. At the downstream end of the river (Catchment Z), we predict a relatively high erosion rate from the mixing model but a relatively low concentration of young ages in comparison to the other catchments. This could mean that, in catchment Z, the present-day high erosion rate is relatively recent and has not led yet to a complete resetting of cooling ages which were set during earlier events.

5   We also note (Table 3 and Figure 6) that all erosion rate distributions predicted by the bootstrapping method are highly asymmetrical, as the median value is always significantly smaller than the mean. The standard deviation is large, of the order of 30-50% of the mean value or 50-100% of the modal value of predicted erosion rate values. Interestingly, the standard deviation does not increase downstream which demonstrates that the uncertainty introduced by using incomplete or non-representative sub-samples of the true distributions at each of the station does not accumulate as our algorithm proceeds from station to
10   station. This results from the incremental nature of our algorithm, as shown by Equation 11.

       One of the main source of error/uncertainty in our estimates of the erosion rate comes from the assumed value of the lithological factors, α_i, which might be difficult to estimate in many situations. We can compute the uncertainty on the erosion rates, $\Delta\epsilon_i$ arising from the uncertainty on the lithological factors, $\Delta\alpha_i$, from:

$$\Delta\epsilon_i = \sqrt{\sum_{k=1}^{i}\left(\frac{\partial\epsilon_i}{\partial\alpha_k}\right)^2\Delta\alpha_k^2} \qquad (29)$$

15   where:

$$\frac{\partial\epsilon_i}{\partial\alpha_k} = \left\{ \begin{array}{ll} 0 & \text{if } k > i \\ \frac{\epsilon_i}{\alpha_i} & \text{if } k = i \\ \frac{\delta_i}{A_i\alpha_i}\left(A_k\epsilon_k + \sum_{j=1}^{i-1}A_j\alpha_j\frac{\partial\epsilon_j}{\partial\alpha_k}\right) & \text{if } k < i \end{array} \right\} \qquad (30)$$
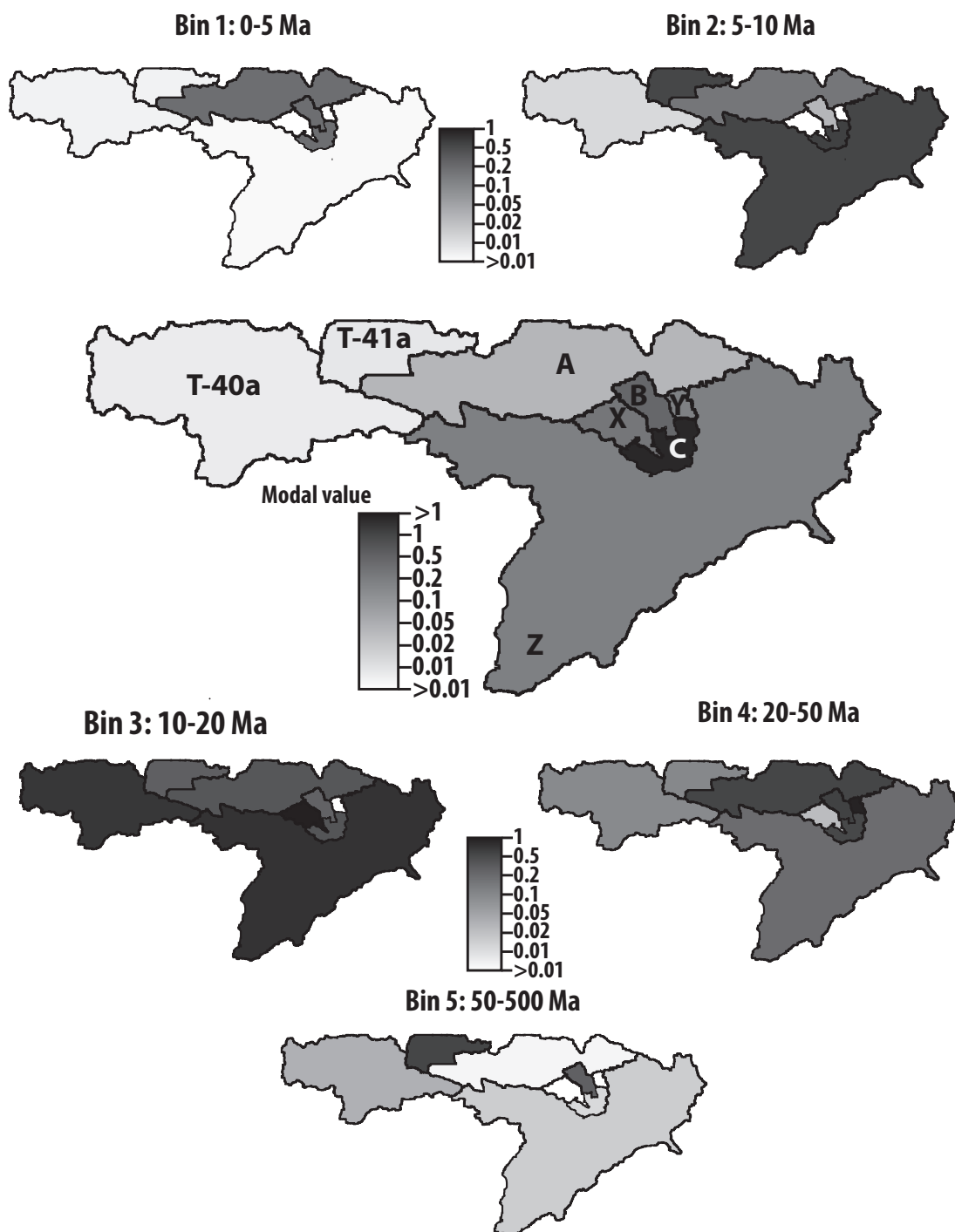
Figure 5. Predicted modal erosion rates (central panel) and relative surface age concentration from the Muscovite detrital data from Eastern Himalaya. See Figure (4) for data distribution.
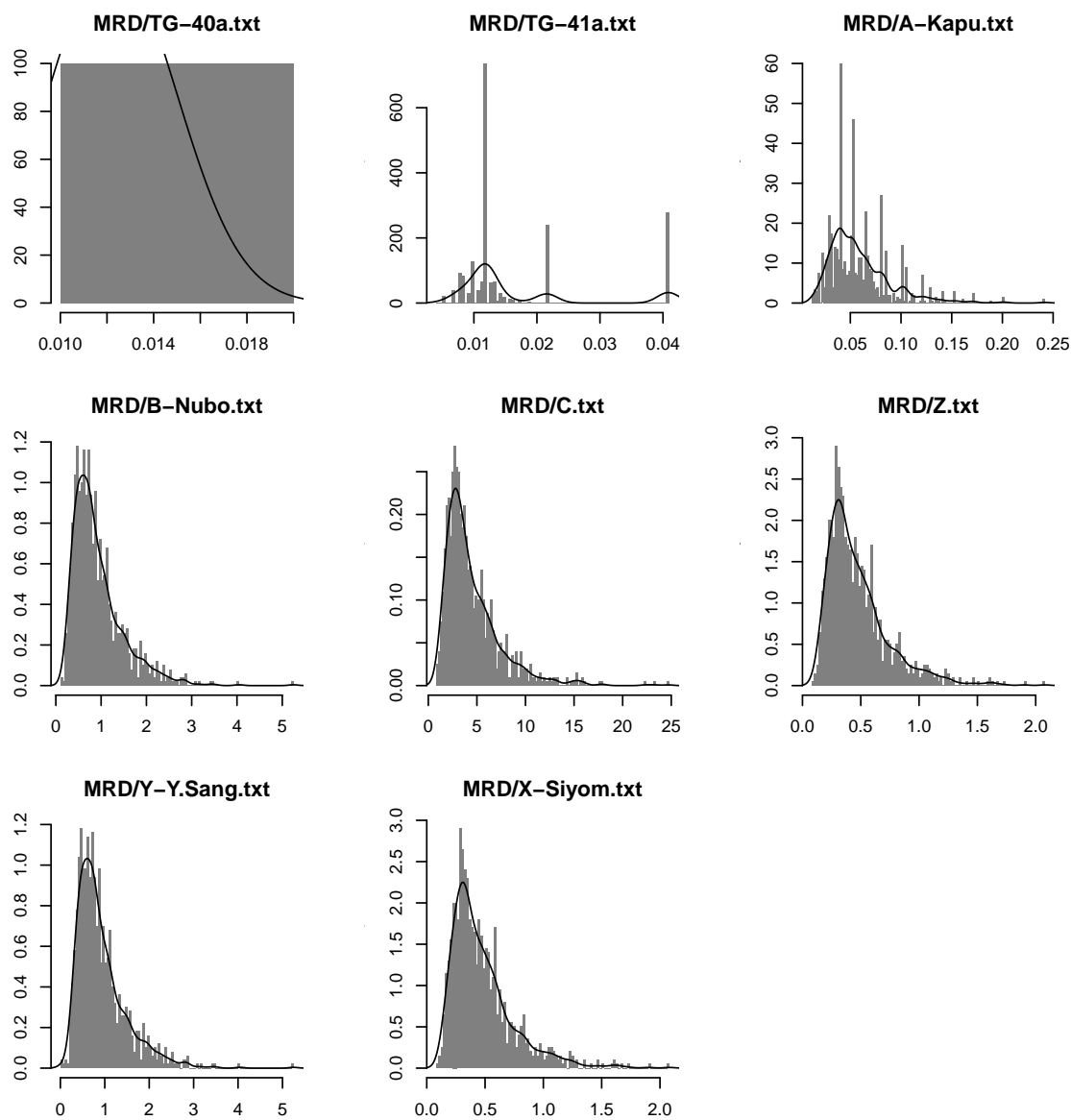
Figure 6. Distributions of predicted present-day erosion rate in mm/yr as derived by bootstrapping. See Figure (4) for sites locations.

The results are shown in Figure 7 as a plot of the ratio between the relative uncertainty in estimates of erosion rate $\Delta\epsilon_i/\epsilon_i$ and the relative uncertainty in lithological factors, $\Delta\alpha_i/\alpha_i$, for the six stations located along the main river trunk. We see that the relative uncertainty in erosion rate is approximately proportional to the relative uncertainty in lithological factor (i.e. all values are close to 1) and that there is only a minor downstream propagation of the uncertainty . This is also a simple consequence of

5   the incremental nature of our algorithm, as explained by Equation 11.
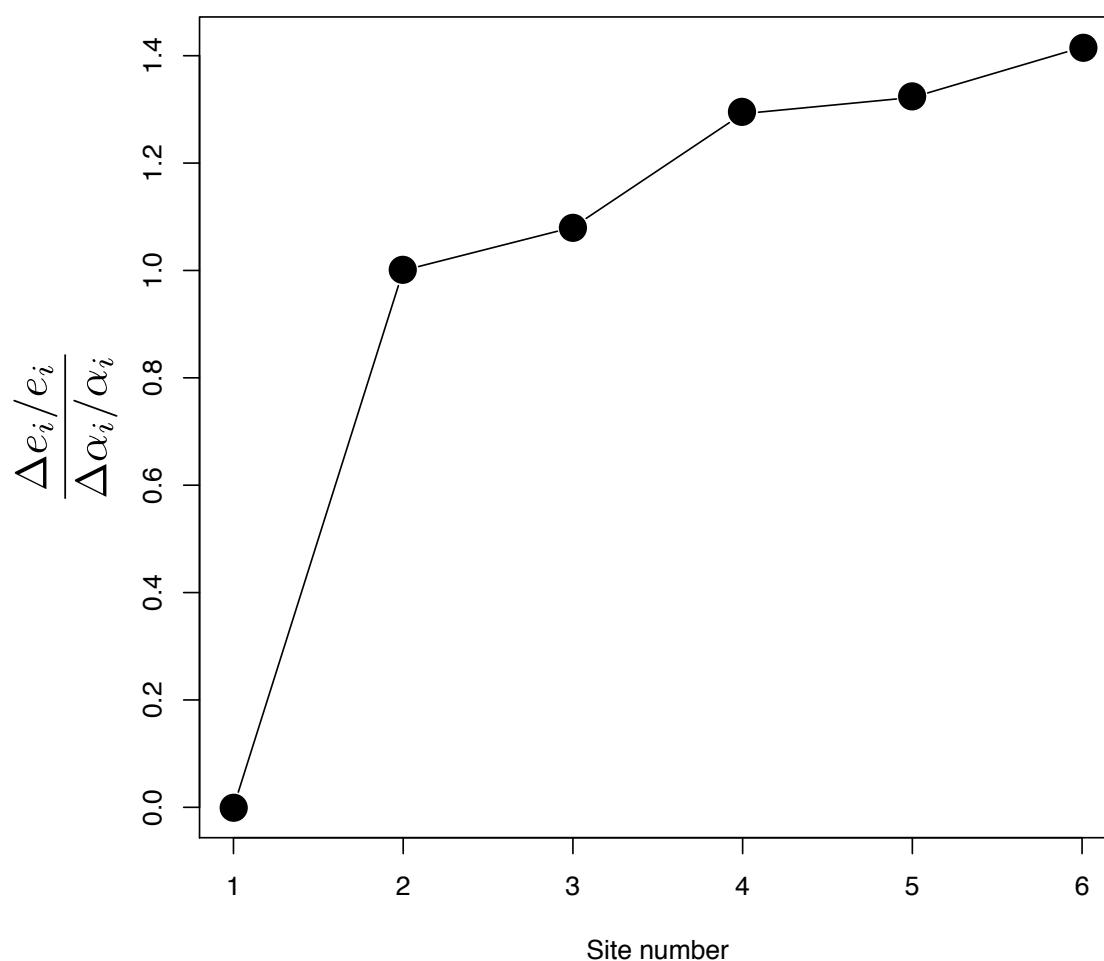
Figure 7. Relative uncertainty in erosion rate scaled by the relative uncertainty in lithological factor for the estimates obtained at each of the six sites along the main river trunk. The first site has a fixed erosion rate and therefore no uncertainty.

6 Conclusions

We have developed a simple method to extract spatially variable erosion rates and surface age distributions from detrital cooling age datasets from modern river sands. The method is based on what we believe are the simplest assumptions necessary to interpret such data. In describing the method we demonstrate that it is well suited to extract from detrital cooling age datasets

5 two seemingly independent sources of information pertaining to the spatial distribution of present-day erosion rate along the river. By applying the method to an existing dataset from the eastern Himalaya, we show that the method provides estimates of present-day erosion rate patterns in the area, potentially evidencing that the fast present-day erosion rates in some parts of the study area are relatively young. Importantly, the method is limited to providing the spatial distribution of erosion rate; independent information is necessary to transform those into absolute estimates of erosion rate.

10 *Code and data availability.* We provide a simple implementation of the method in R.code within a Jupyter Notebook that includes the data used in this paper for illustration purposes.

Competing interests. The authors declare that they have no conflict of interest.

Acknowledgements. The work leading to the results presented here was supported by the People Programme (Marie Curie Actions) of the European Union's Seventh Framework Programme FP7/People/2012/ITN, Grant agreement number 316966.

References

Bernet, M., Brandon, M., and Garver, J. I. (2004). Downstream changes of Alpine zircon fission-track ages in the Rhône and Rhine Rivers. *J. Sed. Res.*, 74:82–94.

Bracciali, L., Parrish, R. R., Najman, Y., Smye, A., Carter, A., and Wijbrans, J. R. (2016). Plio-Pleistocene exhumation of the eastern Himalayan syntaxis and its domal 'pop-up'. *Earth Sc. Rev.*, 160(C):350–385.

Brandon, M. (1992). Decomposition of fission-track grain-age distributions. *Am. J. Sci.*, 292:535–564.

Braun, J. (2016). Strong imprint of past orogenic events on the thermochronological record. *Tectonophysics*, 683:325–332.

Brewer, I. D., Burbank, D. W., and Hodges, K. V. (2006). Downstream development of a detrital cooling-age signal: Insights from 40Ar/39Ar muscovite thermochronology in the Nepalese Himalaya. In *Special Paper 398: Tectonics, Climate, and Landscape Evolution*, pages 321–338. Geological Society of America.

Brown, R. (1991). Backstacking apatite fission track "stratigraphy": a method for resolving the erosional and isostatic rebound components of tectonic uplift histories. *Geology*, 19:74–77.

Dodson, M. (1973). Closure temperature in cooling geochronological and petrological systems. *Contrib. Mineral. Petr.*, 40:259–274.

Enkelmann, E. and Ehlers, T. A. (2015). Evaluation of detrital thermochronology for quantification of glacial catchment denudation and sediment mixing. *Chemical Geology*, 411(C):299–309.

Gleadow, A. and Brooks, C. K. (1979). Fission track dating, thermal histories and tectonics of igneous intrusions in East Greenland. *Contributions to Mineralogy and Petrology*, 71(1):45–60.

Hames, W. and Bowring, S. (1994). An empirical evaluation of the argon diffusion geometry in muscovite. *Earth Planet. Sc. Lett.*, 124:161–169.

Lang, K. A., Huntington, K. W., Burmester, R., and Housen, B. (2016). Rapid exhumation of the eastern Himalayan syntaxis since the late Miocene. *Geol. Soc. Am. Bull.*, 128:1403–1422.

Malusà, M. G., Resentini, A., and Garzanti, E. (2016). Hydraulic sorting and mineral fertility bias in detrital geochronology. *Geol. Rundsch.*, 31:1–19.

McPhillips, D. and Brandon, M. (2010). Using tracer thermochronology to measure modern relief change in the Sierra Nevada, California. *Earth Planet. Sc. Lett.*, 296:373–383.

Ruhl, K. W. and Hodges, K. V. (2005). The use of detrital mineral cooling ages to evaluate steady state assumptions in active orogens: An example from the central Nepalese Himalaya. *Tectonics*, 24(4):TC4015, doi:10.1029/2004TC001712.

Stock, G. M., Ehlers, T. A., and Farley, K. A. (2006). Where does sediment come from? Quantifying catchment erosion with detrital apatite (U-Th)/He thermochronometry. *Geology*, 34(9):725–728.

Vermeesch, P. (2007). Quantitative geomorphology of the White Mountains (California) using detrital apatite fission track thermochronology. *J. Geophys. Res.*, 112(F3):FO3004.

Whipp, D. M., Ehlers, T. A., Braun, J., and Spath, C. D. (2009). Effects of exhumation kinematics and topographic evolution on detrital thermochronometer data. *J. Geophys. Res.*, 114(F4):F04021.

Wobus, C. W., Hodges, K. V., and Whipple, K. X. (2003). Has focused denudation sustained active thrusting at the Himalayan topographic front? *Geology*, 31:861864.

Wobus, C. W., Whipple, K. X., and Hodges, K. V. (2006). Neotectonics of the central Nepalese Himalaya: Constraints from geomorphology, detrital 40Ar/ 39Ar thermochronology, and thermal modeling. *Tectonics*, 25(4):TC4011.